Desalination and Water Treatment
www.deswater.com

doi: 10.1080/19443994.2016.1179675

57 (2016) 28496–28511
December

Taylor & Francis
Taylor & Francis Group

Microwave-assisted regeneration of spent activated carbon containing zinc acetate and its application for removal of congo red

Wenwen Qu[a,b,c,d,e,*], Qiong Hu[b,c,d,e], Yi Zhu[b,c,d,e], Jinhui Peng[b,c,d,e], Libo Zhang[b,c,d,e]

[a]*Faculty of Science, Kunming University of Science and Technology, No. 727, South Jingming Rd., Chenggong District, Kunming 650500, China, Tel. +86 13708806292; email: qwwen77@163.com (W. Qu)*
[b]*Key Laboratory of Unconventional Metallurgy, Ministry of Education, Kunming University of Science and Technology, Kunming 650093, China, Tel. +86 15912106900; email: 375660544@qq.com (Q. Hu), Tel. +86 18314341187; email: 1037425444@qq.com (Y. Zhu), Tel. +86 0871 65916399; email: jhpeng@kmust.edu.cn (J. Peng), Tel. +86 13888310177; email: 942072957@qq.com (L. Zhang)*
[c]*Yunnan Provincial Key Laboratory of Intensification Metallurgy, Kunming University of Science and Technology, Kunming 650093, China*
[d]*National Local Joint Laboratory of Engineering Application of Microwave Energy and Equipment Technology, Kunming University of Science and Technology, Kunming 650093, China*
[e]*State Key Laboratory of Complex Nonferrous Metal Resources Clean Utilization, Kunming University of Science and Technology, Kunming 650093, China*

Received 11 December 2015; Accepted 12 April 2016

ABSTRACT

The spent activated carbon (AC) loaded with zinc acetate from the vinyl acetate synthesis industry has been used as a raw material to prepare AC-ZnO porous adsorbents using microwave irradiation technique with three different activating agents. The morphology and surface chemical compositions of the prepared samples were characterized by X-ray diffraction, scanning electron microscope, Fourier transform infrared spectroscopy, and N_2 adsorption–desorption isotherm. The regenerated AC-ZnO composites exhibited a well-developed porous structure with Brunauer–Emmett–Teller surface area in excess of 1,100 m^2/g, and the ZnO nanoparticles decomposed from zinc acetate loaded on the surface of the regenerated AC without aggregation. The adsorption performance of the AC-ZnO composites was further evaluated by adsorbing Congo Red (CR) from aqueous solutions. The experimental isotherms data were analyzed using Langmuir, Freundlich, and Temkin models. Langmuir and Temkin models were found to satisfactorily match the experimental data with the maximum CR adsorption capacity of 16.72 mg/g for the sample activated by CO_2 at 308 K. Similarly, the kinetics of adsorption were tested with pseudo-first-order, pseudo-second-order, and intraparticle diffusion models, and the data were found to conform to the pseudo-second-order kinetics with high correlation coefficient. The intraparticle diffusion model indicated external film diffusion, and intraparticle diffusion has taken place during the adsorption process.

Keywords: Spent catalyst; Regeneration; AC-ZnO composites; Adsorption; Congo red; Microwave

*Corresponding author.

1. Introduction

In recent years, human survival and development face the challenges of increasingly serious environmental pollution. Effluents with dyes from printing and textile industries are of major threat to environment and human health [1,2]. Most dyes are toxic, non-biodegradable, and tend to trigger several diseases in human beings due to their potential mutagenic or carcinogenic effects. In addition, the presence of dyes in water reduces the light penetration and oxygen absorption necessary for aquatic life, resulting in the gradual destruction of aquatic ecosystems. Thus, it is of great importance to remove the dyes from the industrial wastewater before discharge.

Various treatment techniques, such as membrane filtration [3], ion exchange [4], coagulation [5], electrolysis [6], chemical oxidation [7], solvent extraction [8], etc. are being employed to remove dyes from the wastewater. However, applications of these techniques are associated with disadvantages such as generation of hazardous by-products, energy intensive, and uneconomical. Adsorption is generally accepted as an economical, effective, and easily operated process for the removal of dyes from aqueous solutions [9–11]. Some of the popular adsorbents that were attempted for application in wastewater treatment include zeolite [12], silica [13], red mud [14], and activated carbon (AC) [15], etc. Among them, AC is considered to be most popular due to its large surface area, high adsorption capacity, and organophilic character for organic compounds. However, the high cost of commercially available AC limits its use in most developing countries. In order to solve the problem, many researchers have prepared AC from industrial and agricultural wastes such as sewage sludge [16], tires [17], coir pith [18], *Myrtus communis*, and pomegranate [19], tire crumbs [20], date pits [21], apricot stones [22], walnut shells [23], and wood sawdust [24] for the removal of organic compounds or dyes from aqueous solution. While the conversion of various industrial and agricultural wastes into AC provides a potentially cheap alternative to existing commercial carbons, there is still a great need to prepare AC from cheaper and readily available materials for the removal of dyes from wastewater in pilot and industrial scales.

Recently, increasing emphasis has been placed on the development of processes for regeneration of spent AC as it is considered a solid waste subjected to environmental regulations [25]. Reutilization of spent AC through reactivation on one hand would reduce the solid waste handling cost, on the other hand, would minimize resource utilization, through reduction in the fresh AC consumption. The techniques of regenerating spent AC could be thermal regeneration [26], biological regeneration [27], ultrasonic regeneration [28], and chemical regeneration [29]. Among the above methods, thermal regeneration has been widely adopted owing to the ability to produce AC with desirable porosity and physical characteristics. Unfortunately, the conventional thermal regeneration technique has some drawbacks such as long processing time and high energy consumption. Microwave heating is recognized as a promising technique for the regeneration of AC due to its ability to rapidly increase temperature by dielectric heating [30]. In contrast to conventional heating methods relying on conduction and convection principles, microwave irradiation produces efficient internal ''in core'' volumetric heating by direct coupling of microwave energy with the molecules that are present in the reaction mixture [31]. Therefore, microwave irradiation raises the temperature of the whole reaction mixture simultaneously, resulting in higher yield and purity of products in comparison with conventional methods. In fact, microwave heating technology has been applied successfully for fast regeneration of industrial waste AC and indicated promising results in removal of organic pollutants from aqueous solution [32,33]. For instance, X. Duan et al. [34] regenerated spent coal-based AC from the silicon industry by microwave heating and reported its potential for the removal of Methylene Blue dyes. Mao et al. [35] compared the difference between constant power and constant temperature on microwave regeneration of toluene and acetone saturated AC from agricultural residue. Application of microwave heating technology from cheaper and renewable sources for industrial production of AC-based adsorbents is of high commercial interest.

Vinyl acetate is one of the largest produced organic chemicals as it is the precursor for poly vinyl alcohol and acetals. In China, around 10,000 tons of spent catalysts containing zinc acetate were generated from vinyl acetate synthesis as solid waste every year. The spent catalyst is mainly composed of granular AC and zinc acetate, which is a valuable secondary resource for preparation of AC-based absorbents. However, there are few reports on the utilization of the spent catalyst and the present methods for recovering the AC by leaching zinc from the spent catalyst with acidic or base solutions are easy to produce secondary pollution and are not commercially available [25,36]. Furthermore, the zinc acetate contained in spent catalysts can be decomposed into ZnO, which is a commonly used photocatalyst for degradation of organic compounds. In a word, the synergistic effect can strengthen the adsorption and degradation performance of materials.

The present investigation depicts the development of a simple and fast method for microwave regenerating spent catalyst from vinyl acetate synthesis industry as AC-ZnO porous adsorbents with steam, CO_2, and steam–CO_2 mix gas activation. In order to investigate the adsorption performance of AC-ZnO composites, CR (1-nepthalene sulfonic acid, 3,3´-(4,4´-biphenylenebis(azo))bis(4-amino-) disodium salt) is selected as a model pollutant because it is the first synthetic dye of anionic azo dyes used in textile industry and it is difficult to be removed from wastewater due to its structural stability and high solubility in aqueous solution. Until now, little work has been performed on removal of CR using regenerated AC [37]. In this study, we have investigated the adsorption performance of regenerated AC-ZnO composites for CR from aqueous solution. Batch adsorption experiments were carried out under different conditions. The experimental data were analyzed using the Langmuir, Freundlich, and Temkin models and kinetics was also discussed using pseudo-first-order, pseudo-second-order, and intraparticle diffusion models in order to obtain a better understanding of the adsorption mechanism of CR in this porous adsorbent.

2. Experimental

2.1. Materials

The spent catalysts loaded with zinc acetate were obtained from a chemical factory, which produce vinyl acetate in Yunnan Province of China. The chemical composition of the spent catalysts is listed in Table 1.

Prior to preparation of AC-ZnO, the spent catalyst was washed several times with distilled water to ensure the removal of the impurities and that the pH was neutral. The other materials were directly used without further purification.

2.2. Preparation of the AC-ZnO Composites

The regenerated experiments were carried out in a self-made microwave tubular furnace, which has a single-mode continuous controllable power and microwaves propagation in a TE10 mode. As shown in Fig. 1, the microwave frequency was 2.45 GHz, while the output power could be set to a maximum of 3,000 W. The activation temperature is controlled by the input microwave power during the activation process, which is measured by nichrome–nickel silicon armor-type thermocouple (the dimension of 8 mm diameter and a length of 450 mm, with the temperature range of 0–1,250˚C), placed such that it touched the material [34]. Two thermocouples have been used to take the average temperature as the final treatment temperature since it is more reliable to represent the real temperature of the reaction mixture. Three experimental series employing steam, CO_2, and CO_2–steam mix gas as activating agents were carried out to investigate the effect of regenerated temperature, time, and the flow rate of activating agents on the porous structure and adsorption capacity of the regenerated AC-ZnO composites. First, the washed spent catalysts were dried at 105˚C in an air oven to complete dryness. Then, 25 g of dried spent catalysts was placed inside a ceramic tube (the inner diameter of 80 mm and the length of 900 mm), and the ceramic tube was placed into the microwave tube furnace. In the regeneration process, the samples were heated to the desired experimental temperature using nitrogen flow as shielding gas. Once it attained the desired activation temperature, the nitrogen flow was terminated and switched to activation flow (steam, CO_2, or CO_2–steam mix gas). The completion of experiment was marked by termination of activating agent and reintroduction of nitrogen flow until the samples were cooled to the room temperature.

The regeneration processes were optimized by response surface methodology adopting a central composite rotatable design, and the details of the optimization process have been reported in our earlier publications [38]. The optimized process conditions for steam were identified to be a regeneration temperature of 850˚C, duration of 35 min, and steam flow rate of 0.6 ml/min, for CO_2 was regeneration temperature of 800˚C, duration of 30 min, and CO_2 flow rate of 600 ml/min, and for steam–CO_2 mix gas was regeneration temperature of 750˚C, duration of 25 min, CO_2 flow rate of 550 ml/min, steam flow rate of 0.5 ml/min. The obtained composites from the optimized process conditions with three different activating agents were used to characterize their surface structure and test as an absorbent for CR removal.

Table 1
Components of the spent catalyst (%)

Element	C	Zn	O	Al	Si	Ca	P
Wt.%	77.31	10.71	7.60	0.39	0.49	0.51	2.99

2.3. Characterization

X-ray diffraction (XRD) measurements were carried out utilizing a D/max-TTR III XRD spectrometer (Rigaku) with Cu Kα line of 0.1541 nm. The morphologies of the prepared AC-ZnO composites were

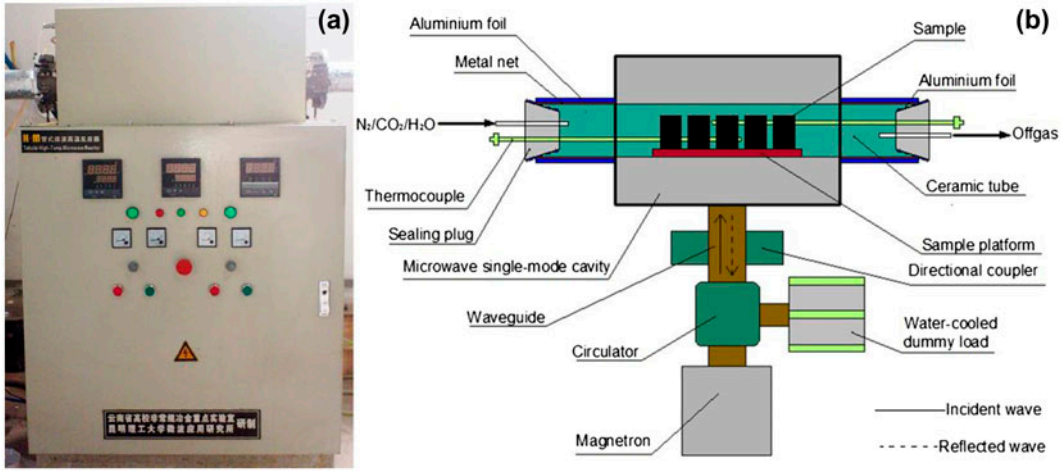

Fig. 1. (a) Picture and (b) schematic illustration of microwave tube furnace.

observed by scanning electron microscope (SEM; Philips XL30 ESEM-TMP). Fourier transform infrared spectroscopy (FT-IR) was carried out utilizing a FTS-40/CC FT-IR spectrometer with 200 mg of KBr. The pore structure characterization of the as-prepared AC-ZnO composites was performed by Autosorb-1-C nitrogen adsorption instrument (Quantachrome). It was performed on the relative pressure from 10^{-7} to 1 Pa and at 77.4 K with high purity nitrogen (99.99%) for the adsorption medium of utilizing volumetric method. The Brunauer–Emmett–Teller (BET) surface area was calculated from the isotherms using the BET equation. While, the pore size distribution (PSD) was determined using non-local density functional theory.

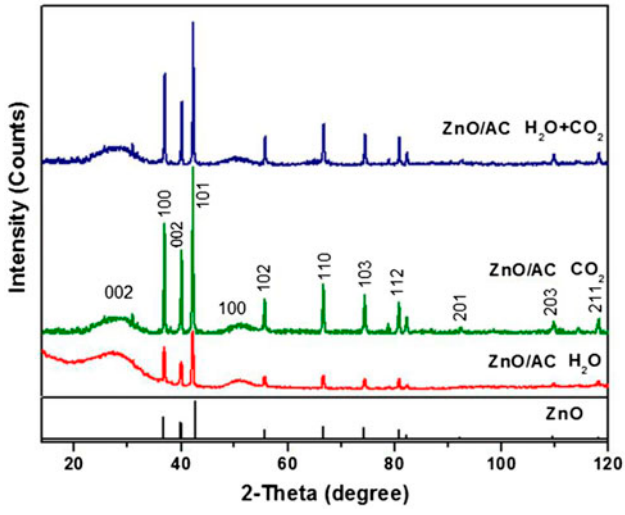

Fig. 2. XRD images of ZnO and AC-ZnO composites activated by steam, CO_2 and steam–CO_2 mix gas.

2.4. Adsorption measurements

The CR number reflects the adsorption capacity of the AC. CR solution was prepared by dissolving calculated amount in distilled water to the desired concentrations. Adsorption experiments were performed in Erlenmeyer flasks (250 ml), each containing 150 ml of different initial concentrations of CR (10–50 mg/L). The concentrations of CR in the supernatant solutions were measured by a spectrophotometer (UV-2550; Shimadzu, Japan) at 488 nm [39] before and after the adsorption process. A small amount of 0.1 mol/L HCl solution was used to adjust the initial pH of the CR solution to 2.7–2.8. At this pH, the dye molecule exists as cations and the active site of AC remains carboxylic (–COOH) and phenolic (Ph–OH). Cationic dye molecules get attached on the surface of AC by replacing H^+ ion of carboxylic and phenolic ions. Therefore, adsorption of CR on the AC surface is much higher at acidic pH than at basic pH [40]. The adsorbed amount of CR under equilibrium condition, q_e (mg/g), was calculated by the following Equation:

$$q_e = \frac{(C_0 - C_e)V}{m} \quad (1)$$

where C_0 and C_e are the initial and equilibrium CR concentrations in solution, respectively (mg/L), V is the volume of the solution (l), and m is the mass (g) of the samples.

The kinetic tests were carried out following the same procedure used for the equilibrium tests. CR solution was taken at different intervals of time and the concentrations of CR were measured at the same intervals. The amount of CR absorbed onto the

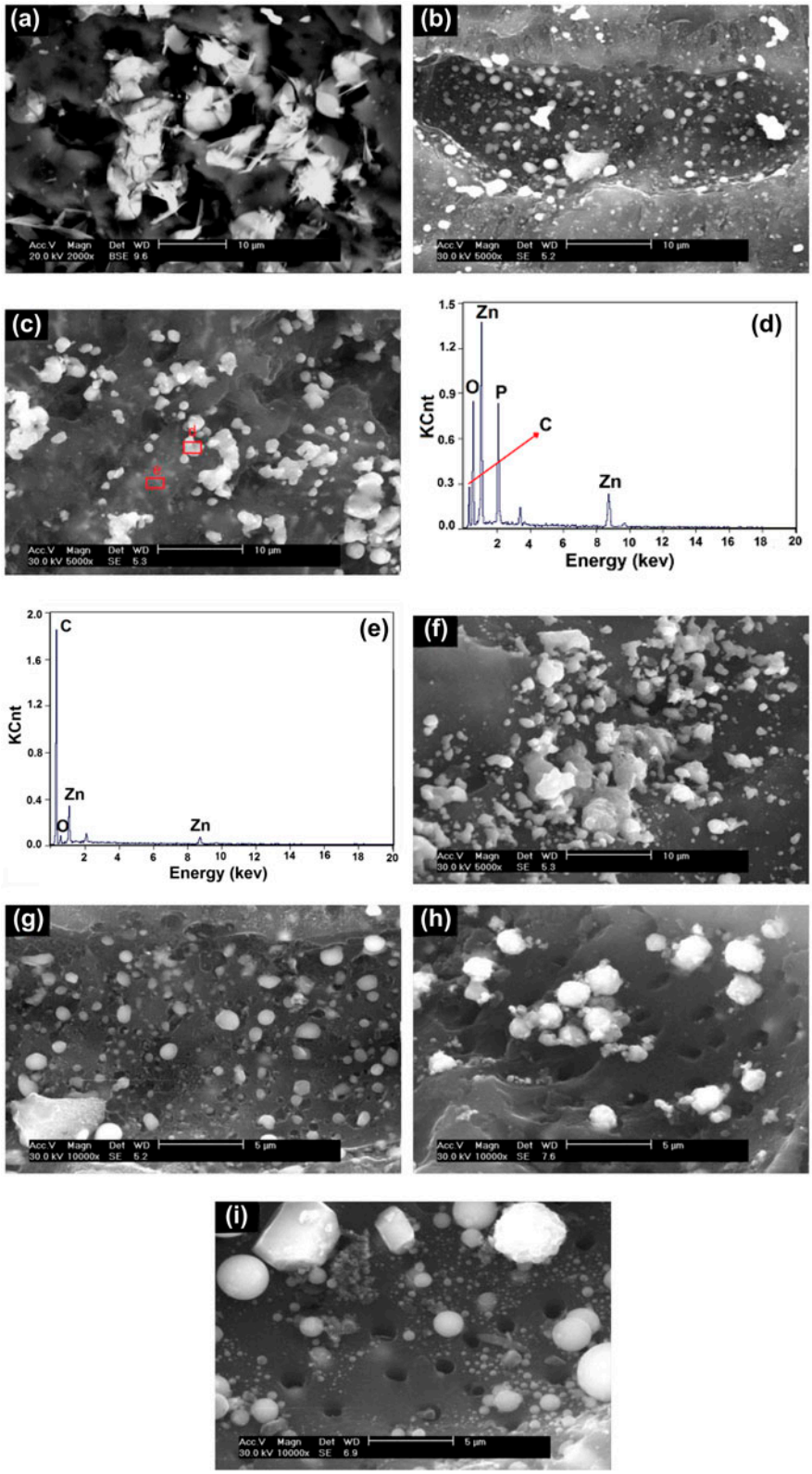

Fig. 3. SEM images of (a) spent catalysts; AC-ZnO composites activated by (b, g) steam; (c, h) CO_2; (f, i) steam-CO_2 mix gas; (d, e) EDX spectra obtained from the areas marked with red circle in (c).

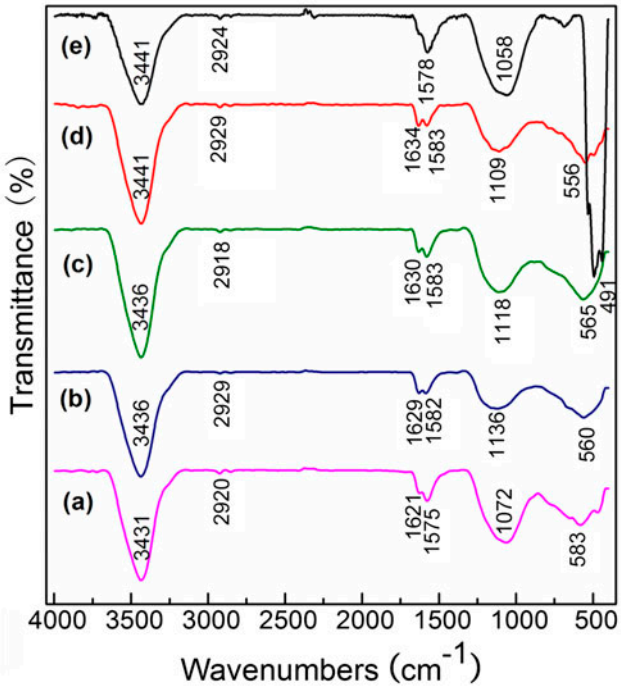

Fig. 4. FT-IR spectra of (a) AC; AC-ZnO composites activated by (b) steam; (c) CO_2 and (d) steam–CO_2 mix gas; (e) pure ZnO.

regenerated samples at time t; q_t (mg/g) was calculated by the following equation:

$$q_t = \frac{(C_0 - C_t)V}{m} \quad (2)$$

where C_0 and C_t are the concentrations at an initial and pre-determined time t (mg/L), respectively, V is the volume of solution (l), and m is the mass (g) of the samples.

3. Results and discussion

3.1. Characteristics of AC-ZnO composites

XRD is one of the most important techniques for characterizing the structure of crystalline or other ordered materials. Fig. 2 shows the XRD patterns of AC-ZnO composites. As is shown in the figure, the 10 diffraction peaks correspond to the characteristic peaks of zinc oxide with wurtzite structure (JCPDS No.36-1451), and the two broad diffraction peaks located near at $2\theta = 26^\circ$ and 44° can be assigned to (0 0 2) and (1 0 0) planes of AC, respectively. The main XRD peak is observed from 37° to 43°, which indicates the zinc acetate decomposition into ZnO with specific shape and size.

Fig. 3 shows the SEM images of the spent catalysts and AC-ZnO samples obtained under different preparation conditions, and the EDX images in Fig. 3(d) and (e) were obtained from the area marked in (c). As seen from Fig. 3(a), the pores of spent catalysts have been blocked by impurities resulting in very minimal availability of pores on the spent catalysts. However, as can be seen from Fig. 3(g), (h), and (k), after being activated, the blocked pores opened as the zinc acetate decomposed along with the removal of other contaminants. In addition, ZnO particles well adhered on the surface of AC, as shown in Fig. 3(b), (c), and (f). The EDX spectra confirming that the composition of regenerated sample mainly corresponds to C and ZnO.

Fig. 4 is the FT-IR spectra of AC, ZnO, and AC-ZnO composites. A wide vibration absorption band of AC (Fig. 4(a)) centered at 3,431 cm^{-1} corresponds to O–H stretching vibration mode of hydroxyl groups, while it moves slightly to higher wave numbers in ZnO and the regenerated AC-ZnO samples. The vibration shifts may be caused by the increase in positive charge on O–H groups adsorbed on the surface of ZnO and AC-ZnO composites, confirming the changes of the acid–base character of the hydroxyl groups in these catalysts. Moreover, the band near at 1,630 and 1,580 cm^{-1} can be assigned to C=C stretching vibration and the aromatic skeletal vibration of AC. The band at around 1,100 cm^{-1} corresponding to a C–O–C stretching vibration can be observed on the surface of AC-ZnO composites. These absorption bands are consistent to that of literature reports [41,42]. At low wave numbers, the band located at about 550 cm^{-1} in Fig. 4(b), (c), and (d) can be assigned to Zn–O stretching vibration absorption of AC-ZnO samples [43], a blue shift appears compared to the strong Zn–O stretching vibration band at 490 cm^{-1} of pure ZnO. The blue shift may be due to the higher vibration couplings of Zn–O in AC-ZnO composites, which is related to the crystallite size and the degree of internal structural ordering.

The nitrogen adsorption isotherm of AC-ZnO samples and spent catalysts at 77 K is shown Fig. 5(a), while the cumulative pore volume is shown in Fig. 5(b), and PSD is shown in Fig. 5(c). From Fig. 5(a), it can be seen that the regenerated products present a high adsorption capacity at relatively low pressures, which indicates the presence of a microporous structure. At relative pressure p/p_0 greater than 0.1, a continued increase in the nitrogen adsorption capacity, possibly indicated a type IV adsorption isotherm under the IUPAC classification of isotherms, which is typical of material with mixture of micro- and mesopores [44]. This is further evidenced by the formation of hysteresis loop which is usually

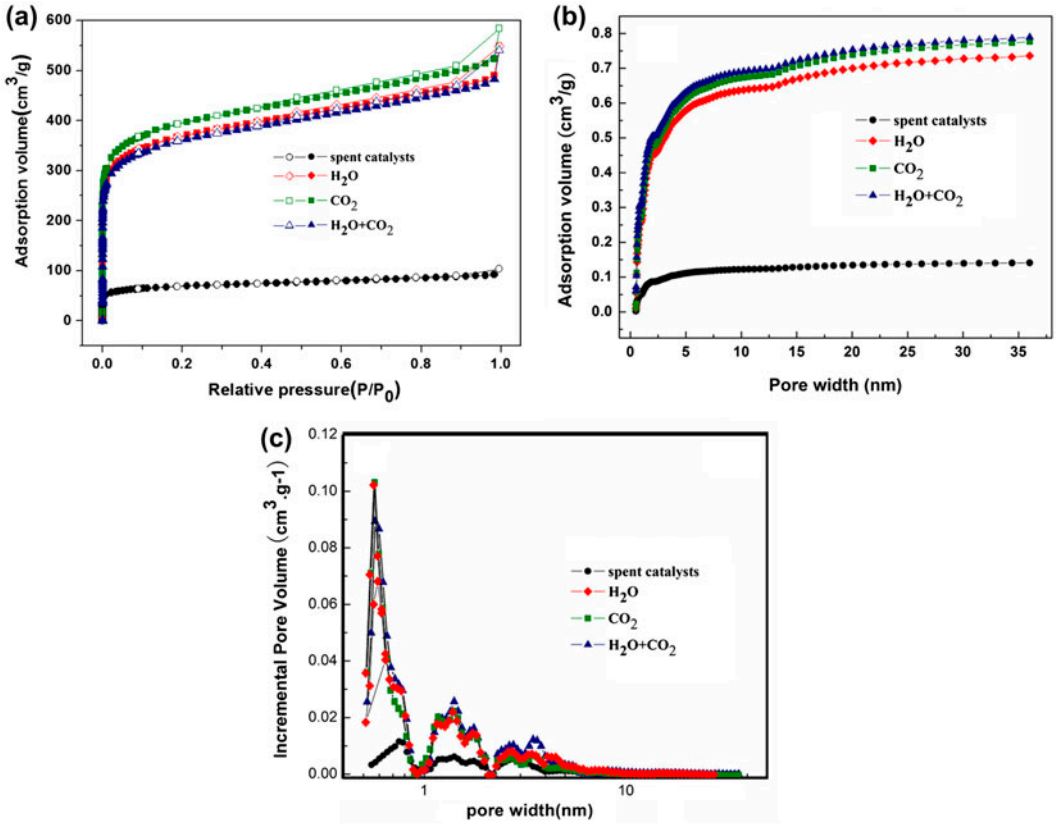

Fig. 5. (a) Nitrogen sorption isotherm (filling symbols: adsorption; no filling symbols: desorption), (b) Cumulative pore volume distribution, and (c) Pore size distribution of spent catalysts and AC-ZnO composites.

Table 2
Textural parameters of the spent catalysts and AC-ZnO composites

Material	Specific surface area (m^2/g)	Total pore volume (cm^3/g)	Average pore diameter (nm)
Spent catalysts	212.6	0.141	2.547
Steam activation	1,109	0.736	2.647
CO_2 activation	1,170	0.776	2.731
Steam–CO_2 activation	1,114	0.739	2.680

associated with the filling and emptying of mesopores [45]. The PSD diagram in Fig. 5(c) indicates that there were a large proportion of pores in the AC-ZnO below 2 nm, which corresponds to the microporous structures. Besides, there are also a few mesoporous structures above 2 nm, although they do not make a great contribution to the BET surface area and total pore volume. The summary of the textural characteristics of the AC-ZnO composites prepared under different conditions is provided in Table 2. Among the three regeneration methods, CO_2 regeneration resulted in a marginally higher pore volume, surface area, and average pore diameter. The enhanced pore volume and surface area in the process of regeneration can be attributed not only to the removal of contaminant from the pores but also to the generation of new pores during the process of activation.

3.2. Adsorption studies

3.2.1. Effects of contact time and initial CR concentrations

Fig. 6 shows the effects of contact time on the adsorption capacity of CR onto AC-ZnO composites at different initial concentrations (10–50 mg/L). As can be seen, the adsorption rates drastically increase during the initial stage due to that most vacant surface

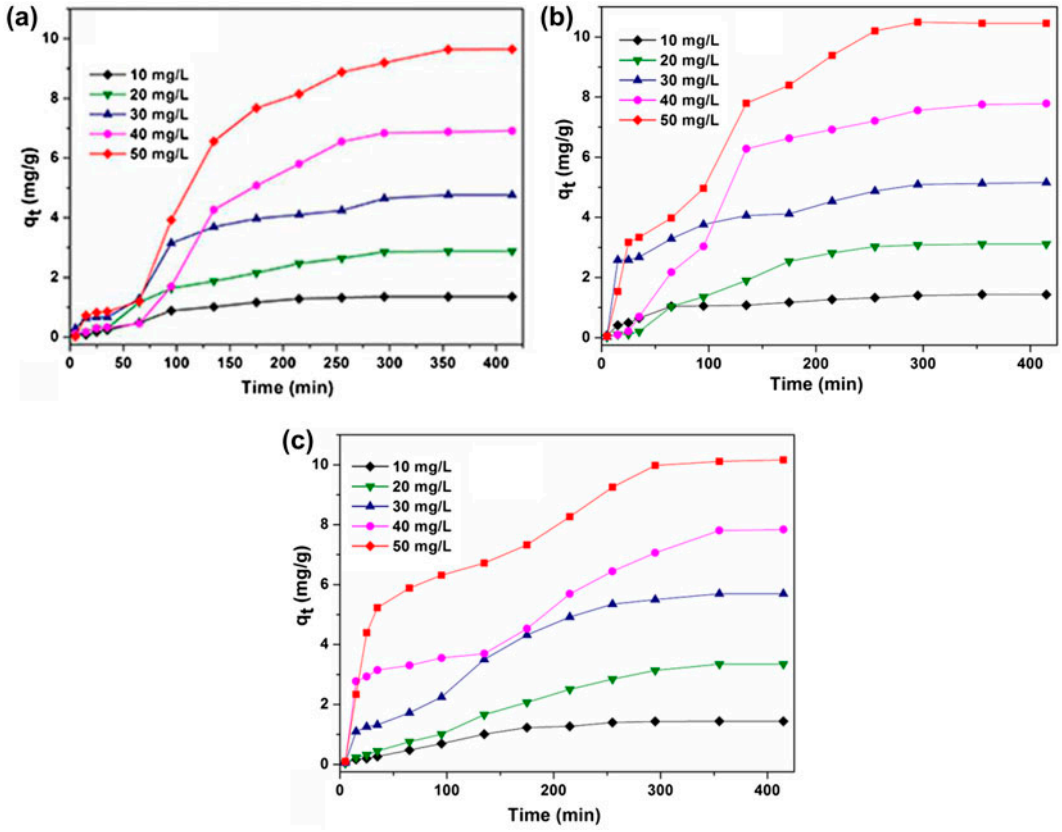

Fig. 6. Effects of contact time on the adsorption capacity of CR onto AC-ZnO composites at different initial concentrations with (a) steam activation, (b) CO_2 activation, and (c) steam–CO_2 mix gas activation at 298 K.

sites are available for adsorption at this time. The equilibrium adsorption capacities increase with increasing initial CR concentrations, since initial CR concentrations can provide a driving force to overcome the mass transfer resistance of CR, thus accelerates the diffusion of CR from the solution onto the adsorbent. The equilibrium time of CR onto composites was 295, 300, and 345 min for steam, CO_2, and joint gas activation, and the equilibrium adsorption capacity (q_e) was 9.65, 10.45, and 10.16 mg/g for steam, CO_2, and steam–CO_2 mix gas activation at room temperature, respectively. In order to analyze the isotherm and kinetics for the adsorption process, three isotherm and three kinetic models were applied.

3.2.2. Adsorption isotherm

The equilibrium adsorption isotherms are fundamental in describing the interaction between the adsorbates and adsorbent and are essential in giving an idea of the adsorption capacity of the adsorbent. Three theoretical models (Langmuir, Freundlich, and Temkin) are used for describing the adsorption behaviors. Their linear functions can be described as follows [46–48]:

$$\text{Langmuir model: } \frac{C_e}{q_e} = \frac{1}{q_m K_L} + \frac{1}{q_m} C_e \quad (3)$$

$$\text{Freundlich model: } \ln q_e = \frac{1}{n} \ln C_e + \ln K_F \quad (4)$$

$$\text{Temkin model: } q_e = B \ln K_T + B \ln C_e \quad (5)$$

In these equation, q_e (mg/g) is the equilibrium amount of CR adsorbed; C_e (mg/L) is the equilibrium CR concentration in solution; K_L (L/mg) and q_m (mg/g) are the Langmuir constants involved in adsorption rate and maximum adsorption capacity; K_F and n are the Freundlich constants, indicating the extent of adsorption and the degree of nonlinearity of adsorption; K_T (L/mg) is the equilibrium binding constant corresponding to the maximum binding energy; B is related to the heat of adsorption. Two deviation tests—the average relative error (ARE) deviation and Marquardt's percent standard deviation (MPSD)—

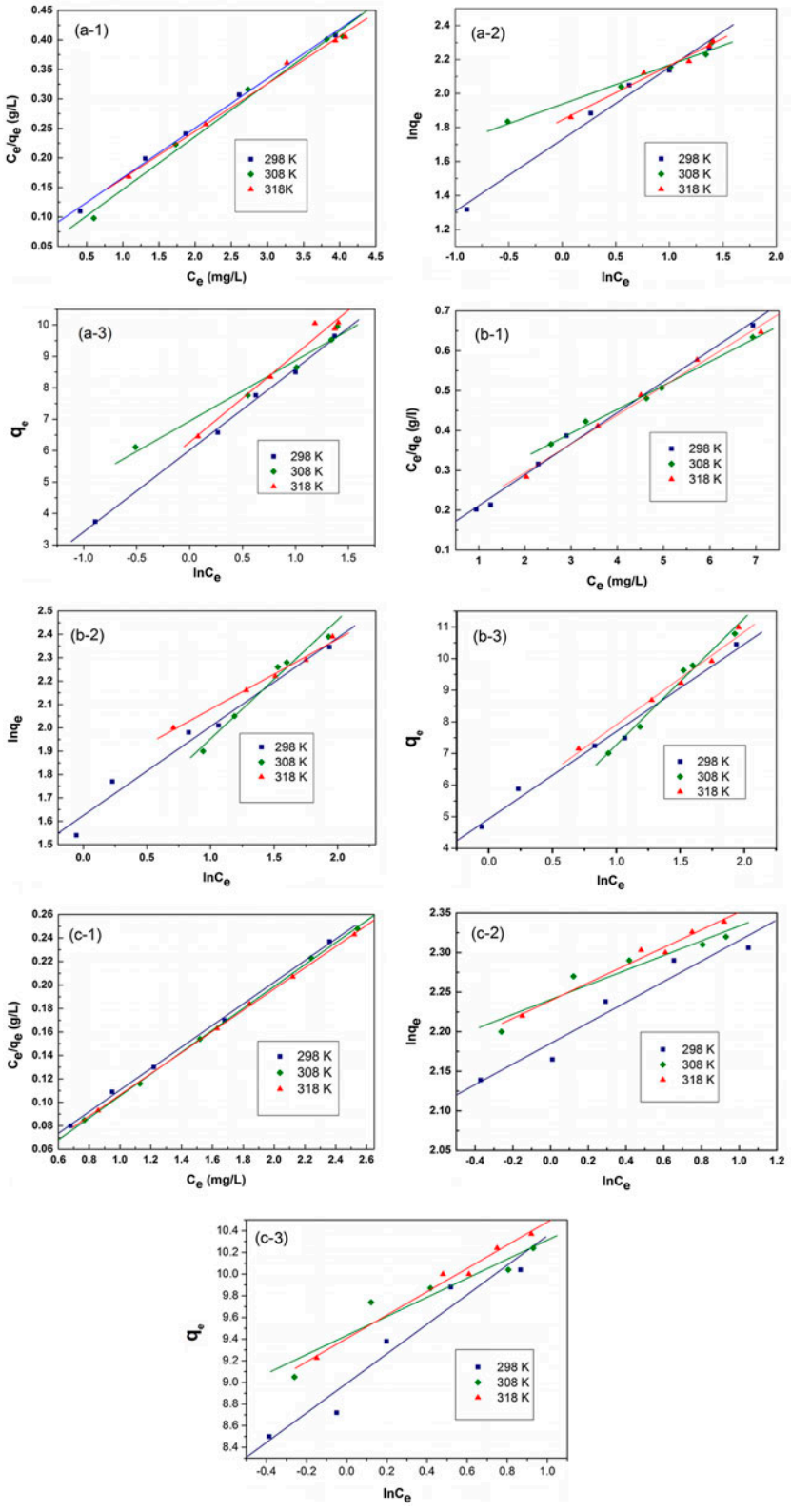

Fig. 7. Langmuir, Freundlich, and Temkin adsorption isotherm of CR onto AC-ZnO composites activated by: (a) steam, (b) CO_2, and (c) steam–CO_2 mix gas.

Table 3
Isotherm parameters for CR adsorption on AC-ZnO composites

Isotherm model		Steam			CO_2			Steam–CO_2		
		298	308	318	298	308	318	298	308	318
Langmuir	q_m (mg/g)	11.91	11.38	12.43	12.86	16.72	13.83	10.87	10.71	11.07
	k_L (L/mg)	1.02	1.58	0.95	0.58	0.28	0.48	4.99	7.67	5.67
	R^2	0.998	0.995	0.997	0.996	0.997	0.995	0.999	1	1
	ARE	2.66	4.95	2.19	4.16	1.60	2.54	1.31	0.81	0.43
	MSPD	7.57	13.77	6.99	11.36	4.06	6.17	3.66	2.07	1.20
Freundlich	$1/n$	0.42	0.23	0.32	0.38	0.51	0.3	0.15	0.09	0.11
	k_F	5.64	6.94	6.33	5.08	4.23	5.92	8.98	9.4	9.39
	R^2	0.993	0.989	0.990	0.987	0.988	0.994	0.970	0.956	0.990
	ARE	3.67	1.72	2.83	3.78	2.90	1.46	1.48	1.18	0.57
	MPSD	8.73	4.54	8.86	9.56	7.31	3.94	3.65	3.11	1.19
Temkin	B	2.60	1.93	2.8	2.76	4.00	2.94	1.36	0.88	1.07
	k_T (L/mg)	10.14	36.49	9.39	5.98	2.26	5.42	734.36	45,264.9	6,276.6
	R^2	0.999	0.987	0.985	0.992	0.992	0.991	0.971	0.951	0.993
	ARE	1.34	2.33	1.94	2.90	1.64	1.49	1.41	1.10	0.43
	MPSE	3.13	5.80	5.38	7.89	4.07	3.90	3.46	2.91	1.09

Table 4
Maximum adsorption capacity (q_m) values for the adsorption of CR on various adsorbents

Adsorbent	q_m (mg/g)	Adsorption isotherms	Refs.
Regenerated AC-ZnO composites from spent catalyst	16.72	Langmuir	This work
Activated carbon prepared from coir pith	6.72	Langmuir and Freundlich	[18]
Activated carbon from *Myrtus communis*	19.23	Langmuir	[19]
Activated carbons from scrap tires	159	Langmuir	[20]
Activated carbon prepared from date pits	105	Langmuir and Redlich–Peterson	[21]
Activated carbon prepared from apricot stones	32.85	Langmuir	[22]
Commercial grade activated carbon	0.64	Langmuir	[51]
Bagasse fly ash	11.88	Freundlich	[51]
Waste red mud	4.05	Langmuir and Freundlich	[52]
Cashew nut shell	5.18	Redlich–Peterson	[53]
Waste banana pith	6.70	Langmuir	[54]
Luffa cylindrical-M	17.39	Langmuir	[55]

were used to investigate the best fit adsorption isotherm, the related equations are as follows [49,50]:

$$\mathrm{ARE} = \frac{100}{n}\sum_{i=1}^{n}\left|\frac{q_{e,exp}-q_{e,cal}}{q_{e,exp}}\right|_i \quad (6)$$

$$\mathrm{MPSD} = 100\sqrt{\frac{1}{n-p}\sum_{i=1}^{n}\left(\frac{q_{e,exp}-q_{e,cal}}{q_{e,exp}}\right)_i^2} \quad (7)$$

where N is the number of experimental data points, $q_{e,cal}$ (mg/g) is the theoretically calculated adsorption capacity at equilibrium, $q_{e,exp}$ (mg/g) is the experimental adsorption capacity at equilibrium, and p is the number of parameters in each isotherm model.

The adsorption isotherms of CR onto AC-ZnO composites were investigated at three different temperatures of 298, 308, and 318 K. The isotherms are shown in Fig. 7(a) (Steam activation), (b) (CO_2 activation), and (c) (Steam–CO_2 mix gas activation), respectively. The model parameters were evaluated and are presented in Table 3, along with the correlation coefficient (R^2), which indicates the suitability of the model with the experimental data. According to Table 3, for steam and CO_2 activation, based on R^2, Langmuir model seems to be more adequate. However, the calculation of the error deviation using both ARE and MPSD revealed that at room temperature, the Temkin model is more suitable to describe the adsorption process by giving lower error estimation values.

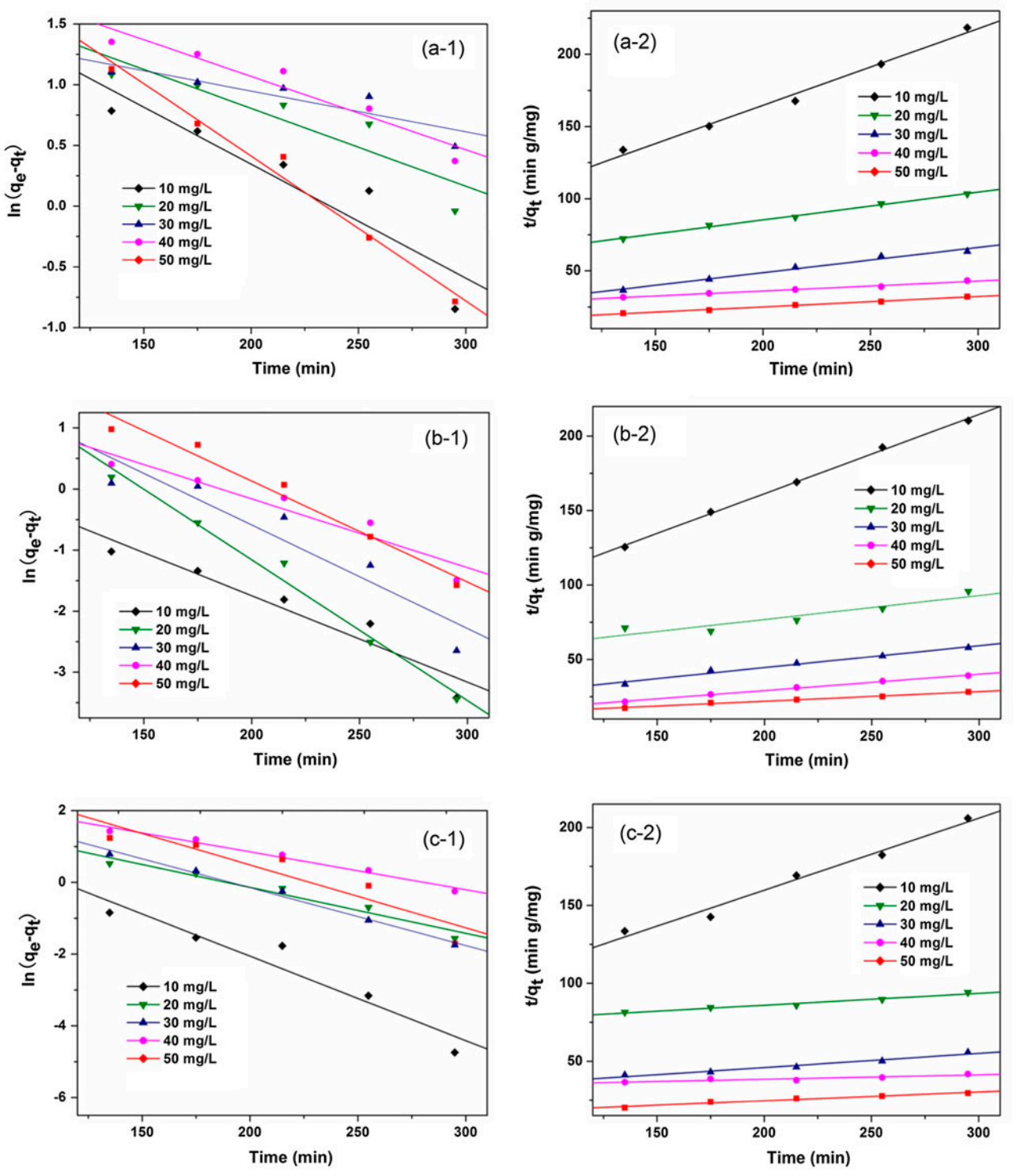

Fig. 8. Pseudo-first-order and pseudo-second-order models of CR onto AC-ZnO composites activated by: (a) steam, (b) CO_2, and (c) steam–CO_2 mix gas.

Table 5
Kinetic models for CR adsorption on AC-ZnO composites

Activating agents	C_0 (mg/L)	First-order kinetic model				Second-order kinetic model		
		q_e (mg/g)	K_1 (min)	$q_{e,cel}$ (mg/g)	R^2	K_2 (min)	$q_{e,cel}$ (mg/g)	R^2
Steam	10	1.35	0.034	60.70	0.93	0.0048	1.89	1
	20	2.87	0.023	37.18	0.91	0.0008	5.17	1
	30	4.76	0.012	6.88	0.89	0.0022	5.73	0.99
	40	6.91	0.022	73.14	0.96	0.0002	14.55	0.99
	50	9.65	0.012	16.42	0.99	0.0005	13.84	1
CO_2	10	1.43	0.014	2.95	0.96	0.0052	1.89	1
	20	3.11	0.023	31.71	0.99	0.0006	6.22	0.93
	30	5.16	0.017	16.43	0.94	0.0015	6.76	0.99
	40	7.78	0.011	8.09	0.96	0.0017	9.08	1
	50	10.45	0.017	31.01	0.98	0.0005	15.5	1
Steam–CO_2	10	1.44	0.024	14.12	0.96	0.0032	2.17	0.99
	20	3.34	0.013	11.17	0.97	0.00008	13.10	0.99
	30	5.70	0.016	21.62	0.99	0.00034	10.83	0.99
	40	7.84	0.011	19.26	0.98	0.00002	35.16	0.91
	50	10.16	0.018	54.53	0.93	0.0002	17.70	0.98

However, as the temperature increases, there exists competition between three models. For steam–CO_2 activation, Langmuir model gives the highest R^2 and the lowest MPSD and ARE, indicating a monolayer adsorption occurring on an energetically uniform surface. For all adsorbents, the maximum adsorption capacity (q_m) calculated from the Langmuir isotherm is 16.72 mg/g and the AC-ZnO adsorbent is activated by CO_2 at 308 K, in this condition, the adsorption of CR onto AC-ZnO composites follows the Langmuir model.

A comparison of the maximum CR adsorption capacity (q_m) of the regenerated ZnO-AC composites with those of other low-cost adsorbents in the literatures is shown in Table 4. It can be seen from the table that the AC-ZnO composites showed the comparable adsorption capacity with respect to other low-cost adsorbents. The maximum adsorption capacity of AC-ZnO composites is slightly lower when compared with the AC prepared from Myrtus communis [19] and apricot stones [22]. However, the adsorption capacity was higher than those of AC prepared from coir pith [18], commercial grade AC [51], Bagasse Fly Ash [51], and other agricultural wastes [53–55]. Therefore, the AC-ZnO composites could also have potential application in removal of dyes from aqueous solutions.

3.2.3. Kinetic studies

Kinetic studies are essential because they provide information for the rate of removal of pollutants from the solution. The kinetics of AC-ZnO composites adsorption were estimated for different initial concentrations of the CR solution, ranging from 10 to 50 mg/L. Fig. 8(a) (Steam activation), (b) (CO_2 activation), and (c) (Steam–CO_2 mix gas activation) is the plot of the adsorption kinetics plotted in accordance with the pseudo-first-order and pseudo-second-order models, respectively. These two kinetic models can be expressed as follows [56,57]:

$$\text{pseudo-first-order model: } \ln(q_e - q_t) = \ln q_e - K_1 t \quad (8)$$

$$\text{pseudo-second-order model: } \frac{t}{q_t} = \frac{1}{K_2 q_e^2} + \frac{t}{q_e} \quad (9)$$

where q_e and q_t (mg/g) represent the amounts of CR adsorbed at equilibrium and any time, respectively. K_1 (min^{-1}) is the rate constant of the pseudo-first-order model and K_2 (mg/g min) is the pseudo-second-order rate constant. The kinetic parameters including correlation coefficients (R^2), K_1, K_2, and calculated $q_{e,cal}$ values are displayed in Table 5. As can be observed, the experimental data were fitted better by pseudo-second-order model than pseudo-first-order model, since the correlation coefficient is obviously higher for the pseudo-second-order model. The calculated values of equilibrium adsorption capacity using pseudo-second-order kinetic equation have smaller deviations with the experimental values than those from pseudo-first-order kinetic equation. This further substantiates

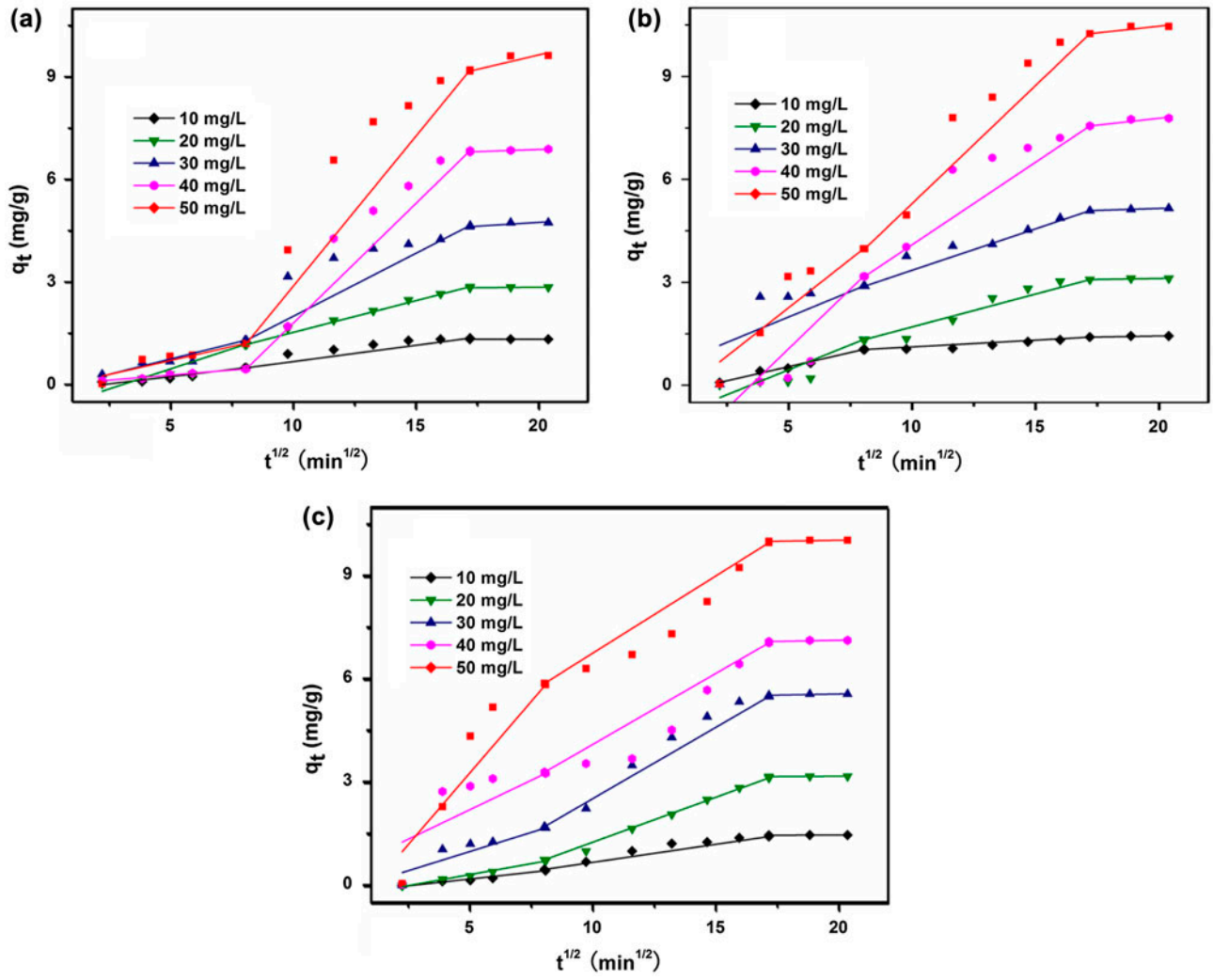

Fig. 9. Intraparticle diffusion kinetic model of CR onto AC-ZnO composites activated by: (a) steam, (b) CO_2, and (c) steam–CO_2 mix gas.

the appropriateness of the use of pseudo-second-order kinetic equation at the present experimental condition.

The steps of adsorption process are studied thoroughly with intraparticle diffusion model which is expressed as [58]:

$$q_t = K_d t^{1/2} + C \tag{10}$$

where K_d (mg/g min$^{1/2}$) is the intraparticle diffusion rate constant and C (mg/g) represents the intercept related to the adsorption steps. The plots of q_t vs. $t^{1/2}$ for the adsorption of CR are shown in Fig. 9. The plots present two distinct regions, indicating that two steps have taken place during the adsorption process. The first region (up to 65 min) is the stage of external film diffusion, which is the diffusion of CR molecules from solution to the external surface of AC-ZnO composites. The second region (65–295 min) is the intraparticle diffusion stage. The fitting correlation coefficients and intraparticle rate constants are presented in Table 6, K_{d1}, K_{d2} are the diffusion coefficient of external film diffusion and intraparticle diffusion, respectively. For steam activation, $K_{d2} > K_{d1}$ suggesting that the intraparticle diffusion had played a more important role in the process of adsorption compared to the external film diffusion. But for CO_2 and steam–CO_2 mix gas activation, K_{d2} was close to K_{d1}, demonstrating that the two stage had competed with each other in the process of adsorption. The results also indicated that intraparticle rate constant increases with increasing in initial concentration.

Table 6
Intraparticle diffusion kinetic model parameters for CR adsorption on AC-ZnO composites

Activating agents	C_0 (mg/L)	K_{d1}	R_1^2	K_{d2}	R_2^2
Steam	10	0.072	0.94	0.089	0.95
	20	0.187	0.91	0.180	1
	30	0.155	0.94	0.30	0.90
	40	0.061	0.99	0.72	0.98
	50	0.184	0.93	0.85	0.96
CO_2	10	0.160	0.99	0.042	0.96
	20	0.166	0.86	0.246	0.98
	30	0.489	0.84	0.188	0.99
	40	0.367	0.90	0.603	0.93
	50	0.689	0.94	0.723	0.97
Steam–CO_2	10	0.0719	0.98	0.107	0.98
	20	0.121	0.99	0.272	1
	30	0.261	0.92	0.447	0.99
	40	0.493	0.81	0.437	0.96
	50	1.024	0.95	0.452	0.97

4. Conclusion

AC-ZnO composites were prepared from the exhausted AC containing ZnO from vinyl acetate synthesis using different activating agents with microwave heating. The structure and surface morphology analyses from XRD and SEM revealed conversion of zinc acetate to zinc oxide and the ZnO particles well adhered on the surface of AC with specific shape and size. The chemical structure of the AC-ZnO composites examined using FT-IR spectroscopy showed the variations in surface functional groups as compared to bare ZnO. The BET surface area and cumulative pore volume of AC-ZnO composites were much higher than that of the spent catalyst, indicating high porosity and excellent adsorption properties. The synthesized AC-ZnO composites were investigated as potential adsorbents for removal of CR in aqueous solutions. The equilibrium adsorption isotherm data generated at three different temperatures were modeled using Langmuir, Freundlich, and Temkin isotherm models. Langmuir and Temkin models were found to match the experimental data better than Freundlich, evidenced through higher correlation coefficient (R^2) and lower error estimation values. The kinetics of adsorption were modeled using pseudo-first-order, pseudo-second-order, and intraparticle diffusion models. The pseudo-second-order model was found to match the experimental data better than the pseudo-first-order. Intraparticle diffusion model indicated two steps have taken place during the adsorption process.

Acknowledgments

The authors would like to express their gratitude to the National Natural Science Foundation of China (Nos. 51562018, 51004059, and 51464024) and the Natural Science Foundation in Yunnan province (No. 14051157) for financial support.

References

[1] S. Khorramfar, N.M. Mahmoodi, M. Arami, H. Bahrami, Oxidation of dyes from colored wastewater using activated carbon/hydrogen peroxide, Desalination 279 (2011) 183–189.
[2] S.D. Marathe, V.S. Shrivastava, Removal of hazardous Ponceau S dye from industrial wastewater using nanosized ZnO, Desalin. Water Treat. 54 (2015) 2036–2040.
[3] J. Zhang, L. Wang, G. Zhang, Z. Wang, L. Xu, Z. Fan, Influence of azo dye-TiO_2 interactions on the filtration performance in a hybrid photocatalysis/ultrafiltration process, J. Colloid Interface Sci. 389 (2012) 273–283.
[4] L. Jordi, S. Josep, L. Joan, Experimental and modeling study of the adsorption of single and binary dye solutions with an ion-exchange membrane adsorber, Chem. Eng. J. 166 (2011) 536–543.
[5] C. Liang, S. Sun, F. Li, Y. Ong, T. Chung, Treatment of highly concentrated wastewater containing multiple synthetic dyes by a combined process of coagulation/flocculation and nanofiltration, J. Membr. Sci. 469 (2014) 306–315.
[6] Y. Sun, G. Wang, Q. Dong, B. Qian, Y. Meng, J. Qiu, Electrolysis removal of methyl orange dye from water by electrospun activated carbon fibers modified with carbon nanotubes, Chem. Eng. J. 253 (2014) 73–77.
[7] O. Türgay, G. Ersöz, S. Atalay, J. Forss, U. Welander, The treatment of azo dyes found in textile industry wastewater by anaerobic biological method and chemical oxidation, Sep. Purif. Technol. 79 (2011) 26–33.
[8] H. Hu, M. Yang, H. Dang, Treatment of strong acid dye wastewater by solvent extraction, Sep. Purif. Technol. 42 (2005) 129–136.
[9] Ö. Demirbaş, Y. Turhan, M. Alkan, Thermodynamics and kinetics of adsorption of a cationic dye onto sepiolite, Desalin. Water Treat. 54 (2015) 707–714.
[10] S. Hashemian, M. Salimi, Nano composite a potential low cost adsorbent for removal of cyanine acid, Chem. Eng. J. 188 (2012) 57–63.
[11] A.Z. Badruddoza, Z.B. Shawon, W.J.T. Daniel, K. Hidajat, M.S. Uddin, Fe_3O_4/cyclodextrin polymer nanocomposites for selective heavy metals removal from industrial wastewater, Carbohydr. Polym. 91 (2013) 322–332.
[12] X. Jin, B. Yu, Z. Chen, J. Arocena, R. Thring, Adsorption of orange II dye in aqueous solution onto surfactant-coated zeolite: Characterization, kinetic and thermodynamic studies, J. Colloid Interface Sci. 435 (2014) 15–20.
[13] N.M. Mahmoodi, A. Maghsoodi, Kinetics and isotherm of cationic dye removal from multicomponent system using the synthesized silica nanoparticle, Desalin. Water Treat. 54 (2015) 562–571.

[14] M. Shirzad-Siboni, S.J. Jafari, O. Giahi, I. Kim, S.M. Lee, J.K. Yang, Removal of acid blue 113 and reactive black 5 dye from aqueous solutions by activated red mud, J. Ind. Eng. Chem. 20 (2014) 1432–1437.
[15] M. Qiu, C. Huang, Removal of dyes from aqueous solution by activated carbon from sewage sludge of the municipal wastewater treatment plant, Desalin. Water Treat. 53 (2015) 3641–3648.
[16] Y. Chen, W. Jiang, L. Jiang, X. Ji, Treatment of dyeing wastewater by activated carbons derived from municipal sewage sludge, Environ. Prog. Sustainable Energy 31 (2012) 585–590.
[17] A.R. Rahmani, G. Asgari, F.B. Askari, A.E. Torbaghan, Adsorption of lead metal from aqueous solutions using activated carbon derived from scrap tires, Fresenius Environ. Bull. 24 (2015) 2341–2347.
[18] C. Namasivayam, D. Kavitha, Removal of Congo Red from water by adsorption onto activated carbon prepared from coir pith, an agricultural solid waste, Dyes Pigm. 54 (2002) 47–58.
[19] M. Ghaedi, H. Tavallali, M. Sharifi, S.N. Kokhdan, A. Asghari, Preparation of low cost activated carbon from Myrtus communis and pomegranate and their efficient application for removal of Congo red from aqueous solution, Spectrochim. Acta Part A 86 (2012) 107–114.
[20] B. Acevedo, C. Barriocanal, I. Lupul, G. Gryglewicz, Properties and performance of mesoporous activated carbons from scrap tyres, bituminous wastes and coal, Fuel 151 (2015) 83–90.
[21] M. Belhachemi, F. Addoun, Adsorption of congo red onto activated carbons having different surface properties: Studies of kinetics and adsorption equilibrium, Desalin. Water Treat. 37 (2012) 122–129.
[22] M. Abbas, M. Trari, Kinetic, equilibrium and thermodynamic study on the removal of Congo Red from aqueous solutions by adsorption onto apricot stone, Process Saf. Environ. Prot. 98 (2015) 424–436.
[23] J. Yang, K. Qiu, Preparation of activated carbons from walnut shells via vacuum chemical activation and their application for methylene blue removal, Chem. Eng. J. 165 (2010) 209–217.
[24] K.Y. Foo, B.H. Hameed, Mesoporous activated carbon from wood sawdust by K_2CO_3 activation using microwave heating, Bioresour. Technol. 111 (2012) 425–432.
[25] Z. Zhang, Z. Zhang, H. Niu, J. Peng, L. Zhang, W. Qu, H. Pan, Effects of microwave pretreatment on zinc extraction from spent catalyst saturated with zinc acetate, Trans. Nonferrous Met. Soc. China 20 (2010) S182–S186.
[26] J. Cho, Y. Kim, S. Jeon, J. Seo, J. Jung, K. Oh, Improvement of thermal regeneration of spent granular activated carbon using air agent: Application of sintering and deoxygenation, Korean J. Chem. Eng. 31 (2014) 1641–1650.
[27] Ö. Aktaş, F. Çeçen, Bioregeneration of activated carbon: A review, Int. Biodeterior. Biodegrad. 59 (2007) 257–272.
[28] J.L. Lim, M. Okada, Regeneration of granular activated carbon using ultrasound, Ultrason. Sonochem. 12 (2005) 277–282.
[29] R. Berenguer, J.P. Marco-Lozar, C. Quijada, D. Cazorla-Amorós, E. Morallón, Comparison among chemical, thermal, and electrochemical regeneration of phenol-saturated activated carbon, Energy Fuels 24 (2010) 3366–3372.
[30] C.O. Oliver Kappe, Microwave dielectric heating in synthetic organic chemistry, Chem. Soc. Rev. 37 (2008) 1127–1139.
[31] C.O. Kappe, How to measure reaction temperature in microwave-heated transformations, Chem. Soc. Rev. 42 (2013) 4977–4990.
[32] D. Xu, F. Cheng, Y. Zhang, Z. Song, Degradation of methyl orange in aqueous solution by microwave irradiation in the presence of granular-activated carbon, Water Air Soil Pollut. 225 (2014) 1–7.
[33] K.Y. Foo, B.H. Hameed, A rapid regeneration of methylene blue dye-loaded activated carbons with microwave heating, J. Anal. Appl. Pyrolysis 98 (2012) 123–128.
[34] X.H. Duan, C.S. Kannan, W.W. Qu, X. Wang, J.H. Peng, L.B. Zhang, Regeneration of microwave assisted spent activated carbon: Process optimization, adsorption isotherms and kinetics, Chem. Eng. Process. 53 (2012) 53–62.
[35] H. Mao, D. Zhou, Z. Hashisho, S. Wang, H. Chen, H. Wang, Constant power and constant temperature microwave regeneration of toluene and acetone loaded on microporous activated carbon from agricultural residue, J. Ind. Eng. Chem. 21 (2015) 516–525.
[36] L. Dbek, Sorption of zinc ions from aqueous solutions on regenerated activated carbons, J. Hazard. Mater. 101 (2003) 191–201.
[37] M.K. Purkait, A. Maiti, S. DasGupta, S. De, Removal of congo red using activated carbon and its regeneration, J. Hazard. Mater. 145 (2007) 287–295.
[38] W. Jin, W.W. Qu, C.S. Kannan, J.H. Peng, X.H. Duan, S.M. Zhang, Process optimization of preparation of ZnO-porous carbon composite from spent catalysts using one step activation, J. Nanosci. Nanotechnol. 5 (2012) 1–9.
[39] J. Li, D.H.L. Ng, P. Song, C. Kong, Y. Song, P. Yang, Preparation and characterization of high-surface area activated carbon fibers from silkworm cocoon waste for congo red adsorption, Biomass Bioenergy 75 (2015) 189–200.
[40] M.K. Purkait, A. Maiti, S. DasGupta, S. De, Removal of congo red using activated carbon and its regeneration, J. Hazard. Mater. 145 (2007) 287–295.
[41] J. Chen, X. Wen, X. Shi, R. Pan, Synthesis of zinc oxide/activated carbon nano-composites and photodegradation of rhodamine B, Environ. Eng. Sci. 29 (2012) 392–398.
[42] Y.M. Li, X. Liu, Activated carbon/ZnO composites prepared using hydrochars as intermediate and their electrochemical performance in supercapacitor, Mater. Chem. Phys. 148 (2014) 380–386.
[43] R. Al-Gaashani, S. Radiman, N. Tabet, A.R. Daud, Effect of microwave power on the morphology and optical property of zinc oxide nano-structures prepared via a microwave-assisted aqueous solution method, Mater. Chem. Phys. 125 (2011) 846–852.
[44] X. Duan, Z. Zhang, C. Srinivasakannan, F. Wang, J. Liang, Regeneration of spent catalyst from vinyl acetate synthesis as porous carbon: Process optimization using RSM, Chem. Eng. Res. Des. 92 (2014) 1249–1256.
[45] E. Yagmur, Preparation of low cost activated carbons from various biomasses with microwave energy, J. Porous Mater. 19 (2012) 995–1002.

[46] H. Radnia, A.A. Ghoreyshi, H. Younesi, G.D. Najafpour, Adsorption of Fe(II) ions from aqueous phase by chitosan adsorbent: Equilibrium, kinetic, and thermodynamic studies, Desalin. Water Treat. 50 (2012) 348–359.
[47] H.Y. Zhu, Y.Q. Fu, R. Jiang, J.H. Jiang, L. Xiao, G.M. Zeng, S.L. Zhao, Y. Wang, Adsorption removal of congo red onto magnetic cellulose/Fe_3O_4/activated carbon composite: Equilibrium, kinetic and thermodynamic studies, Chem. Eng. J. 173 (2011) 494–502.
[48] Z. Cheng, L. Zhang, X. Guo, X. Jiang, T. Li, Adsorption behavior of direct red 80 and congo red onto activated carbon/surfactant: Process optimization, kinetics and equilibrium, Spectrochim. Acta Part A 137 (2015) 1126–1143.
[49] S. Shahmohammadi-Kalalagh, H. Babazadeh, Isotherms for the sorption of zinc and copper onto kaolinite: Comparison of various error functions, Int. J. Environ. Sci. Technol. 11 (2014) 111–118.
[50] S. Kundu, A.K. Gupta, Arsenic adsorption onto iron oxide-coated cement (IOCC): Regression analysis of equilibrium data with several isotherm models and their optimization, Chem. Eng. J. 122 (2006) 93–106.
[51] I.D. Mall, V.C. Srivastava, N.K. Agarwal, I.M. Mishra, Removal of congo red from aqueous solution by bagasse fly ash and activated carbon: Kinetic study and equilibrium isotherm analyses, Chemosphere 61 (2005) 492–501.
[52] C. Namasivayam, D.J.S.E. Arasi, Removal of congo red from wastewater by adsorption onto waste red mud, Chemosphere 34 (1997) 401–417.
[53] P. Senthil Kumar, S. Ramalingam, C. Senthamarai, M. Niranjanaa, P. Vijayalakshmi, S. Sivanesan, Adsorption of dye from aqueous solution by cashew nut shell: Studies on equilibrium isotherm, kinetics and thermodynamics of interactions, Desalination 261 (2010) 52–60.
[54] C. Namasivayam, N. Kanchana, Removal of congo red from aqueous solutions by cellulosic waste banana pith, pertanica, J. Sci. Technol. 1 (1993) 32–42.
[55] V.K. Gupta, D. Pathania, S. Agarwal, S. Sharma, Amputation of congo red dye from waste water using microwave induced grafted Luffa cylindrica cellulosic fiber, Carbohydr. Polym. 111 (2014) 556–566.
[56] C. Wang, J. Zhang, P. Wang, H. Wang, H. Yan, Adsorption of methylene blue and methyl violet by camellia seed powder: Kinetic and thermodynamic studies, Desalin. Water Treat. 53 (2015) 3681–3690.
[57] Z. Chen, J. Zhang, J. Fu, M. Wang, X. Wang, R. Han, Q. Xu, Adsorption of methylene blue onto poly(cyclotriphosphazene-co-4,4′-sulfonyldiphenol) nanotubes: Kinetics, isotherm and thermodynamics analysis, J. Hazard. Mater. 273 (2014) 263–271.
[58] S. Haider, F.F. Binagag, A. Haider, A. Mahmood, N. Shah, W.A. Al-Masry, S.U.D. Khan, S.M. Ramay, Adsorption kinetic and isotherm of methylene blue, safranin T and rhodamine B onto electrospun ethylenediamine-grafted-polyacrylonitrile nanofibers membrane, Desalin. Water Treat. 55 (2015) 1609–1619.